

Influence of Niobium Adding on the Microstructure and Abrasive Wear Resistance of a Heat-Treated High-Chromium Near-Eutectic Cast Iron Alloy

Ismael Nogueira Rabelo de Melo^{a*} , Anderson Edson da Silva^b , Fabrício Gonçalves de Faria^b,
Ivete Peixoto Pinheiro^b , Leonardo Roberto da Silva^b, Roberto Magalhães Paniago^c 

^aInstituto Federal de Educação, Ciência e Tecnologia de Minas Gerais (IFMG), Ibitiré, MG, Brasil.

^bDepartamento de Engenharia de Materiais, Centro Federal de Educação Tecnológica de Minas Gerais, Belo Horizonte, MG, Brasil.

^cUniversidade Federal de Minas Gerais, Departamento de Física, Belo Horizonte, MG, Brasil.

Received: November 02, 2021; Revised: August 19, 2022; Accepted: August 28, 2022

High chromium cast iron (HCCI) with levels around 26% Cr - 2.9% C according to ASTM A 532 IIIA is widely used in systems where high abrasive wear resistance is required. To evaluate the niobium influence, HCCI with 0.5% Nb and 1% Nb additions were melted, besides one without niobium addition of for comparison. For characterization, X-ray diffractometry, scanning electron microscopy (SEM), Vickers microhardness tests, Rockwell C hardness, carbide quantifications, quantification of the retained austenite by Mössbauer spectroscopy, and rubber wheel abrasion test according to procedure A of ASTM G-65 were performed. The results indicated a reduction in the average size, average perimeter, and carbides volumetric fraction (CVF) due to the addition of niobium, also changing the microstructure of the HCCI from eutectic to hypoeutectic. In some regions, NbC_{0.75} carbides formed a coating around M₇C₃ carbides. The 0.5% Nb alloy showed the best performance in the rubber wheel abrasive wear test, with a 37% average volume loss reduction as compared to the sample without niobium addition with a 130N load and 34% with a 45N load. The 0.5% Nb alloy also had the highest content of retained austenite among the investigated alloys.

Keywords: Niobium, High Chromium Cast Iron, Abrasive Wear, Mössbauer Spectroscopy, Dry Sand Rubber Wheel.

1. Introduction

High chromium cast irons (HCCI) have been widely used, especially in the mining sector, to manufacture components involving high demands for resistance to abrasive wear^{1,2}. The high wear resistance is mainly due to (Fe, Cr)₇C₃ carbides surrounded by a predominantly austenitic or martensitic matrix. Factors such as size, shape, and distribution of carbides, heat treatments, presence of alloy elements, and amount of retained austenite influence the wear properties of the material¹⁻³.

HCCI exhibited hypoeutectic, eutectic and hypereutectic microstructures. The hypoeutectic alloys, in as-cast state, displayed austenitic dendrites involved by a eutectic made of austenite and M₇C₃ carbides. The eutectic alloys showed a lamellar structure, which was formed by the eutectic. At last, the hypereutectic alloys exhibited large hexagonal primary carbides involved by the eutectic¹⁻³.

The hypoeutectic alloys have smaller CVF, with carbide content usually below 30%. The eutectic alloy results in CVF around 30%, while the hypereutectic alloys usually present carbide contents above that value. The literature indicates that, in general, the eutectic microstructure results in a higher resistance to abrasive wear¹⁻³.

To obtain maximum hardness and abrasion resistance, martensitic matrix structures must be produced by full heat treatment, however, it's common to find retained austenite in matrices, and this austenite is very unstable and easily transformed to hard martensite upon impact loading or severe abrasive wear. This can be a mixed blessing, with wonderful results under straight abrasive wear or disastrous results under high impact conditions².

The literature indicates that the addition of Nb in these alloys can increase the resistance to abrasive wear through the formation of NbC_x carbides of high hardness (1500 ~3000HV0.05) and favorable morphology⁴⁻⁸ in addition to improving the machinability of the material⁹. However, there are several gaps regarding the performance optimization and the niobium content, in addition to the fact that high levels of this element can make the alloy application unfeasible due to its high acquisition cost.

Several studies^{5,10-13} showed that small concentrations (less than 1%) of Nb can have a beneficial effect on the wear resistance of HCCI⁶. Furthermore, recent authors have shown that 0.5%Nb in HCCI addition can increase the material machinability at rates over 100% in some conditions^{9,14}, encouraging interest in this range.

In this study, the influence of 0.5%Nb and 1%Nb additions on morphology, microstructure, and abrasive wear resistance

*e-mail: ismaelnmelo@gmail.com

in an alloy with 26%Cr and 2.9%C was investigated, showing that 0.5%Nb improved the abrasion wear resistance over 30% both with 130N and 45N load, however, larger additions of niobium without proper carbon correction can shift the eutectic too much to the right, resulting in the formation of a high fraction of proeutectic austenite and reducing the abrasive wear resistance.

2. Experimental Procedure

The raw material used in the metallic load consisted of pieces of a high chromium cast iron rotor (HCCI) ASTM A 532 Class III type A. The niobium additions were carried out at a temperature of $1550^{\circ}\text{C} \pm 50^{\circ}\text{C}$ using a Fe-Nb alloy with a 66%Nb concentration and $19.73\ \mu\text{m}$ average particle size. The time to dissolve Fe-Nb in the liquid metal was 10 minutes. After this period, samples were analyzed for contents check. The melting was carried out in a medium frequency induction manufactured by Inductotherm brand with a 25 kg capacity. According to ASTM A 532 CLASS III type A, three alloys were cast, whose chemical compositions presented in Table 1.

The samples were poured at $1585^{\circ}\text{C} \pm 15^{\circ}\text{C}$ in open cavities measuring $75 \times 25 \times 12.7\text{mm}$ in resin sand molds. The lower surfaces, which were in contact with the sand, were analyzed. The tested surfaces were ground to remove the raw foundry layer and residues, obtaining homogeneous and smooth surfaces.

The samples were first heat-treated by the annealing temperature of 700°C for 2h. The temperature was increased to 1000°C for 5h to destabilize the austenite, cooled in forced-air for quenching, and tempered at 250°C for 2h to transform the austenitic matrix into martensitic^{2,15}.

X-ray diffractometry was performed on a Shimadzu equipment, model: XRD-7000 with a copper anode ($\lambda = 0.154\text{nm}$), scanning angle from 30° to 85° , scanning speed of $2^{\circ}/\text{min}$ and step of 0.02° . The ICDD powder diffraction file (PDF) numbers and ICSD files were used to identify phases are given in Table 2. The martensite phase was identified using a ferrite PDF file, as they have coincident intensity peaks. To analyze the NbC_x carbides stoichiometry, the peaks of the XRD were compared to BDEC - ICSD No. 39755, 63503, 159872, 163741 and 163744.

The optical microscopy was performed in a platinum inverted metallographic microscope, Fortel - IM713, and the scanning electron microscopy (SEM) in a scanning electron microscope Mod. JSM-6510LV-JEOL and EDS Thermo Scientific UltraDry microprobe. The samples were sanded following the order of granulometry 80, 120, 220, 320, 400, and 600 mesh and polished with $9\ \mu\text{m}$, $3\ \mu\text{m}$, and $1\ \mu\text{m}$ diamond paste. The chemical etching was carried out with durations from 5s to 20s with Vilella reagent (1g of

picric acid + 5 ml of hydrochloric acid + 100 mL of ethyl alcohol P.A.).

Vickers microhardness measurements were performed using a Wolpert and Shimadzu optical micro-measurement device with 400x magnification. Ten impressions were made on each constituent of each alloy using a pyramidal square-based diamond penetrator with a 50g load, both for matrix and carbides.

Eighteen Rockwell C hardness measurements were made per alloy in a model RM401/A durometer, IGV brand.

The count, volumetric fraction, average perimeter, total perimeter, and average carbide size were quantified by analyzing ten images of each alloy with 500x magnification generated by SEM. The presented results are eutectic, secondary and NbC_x equivalent measurements carbides. The image analysis program used was Fiji Image J. Particles smaller than $3\ \mu\text{m}^2$ were disregarded for filtering possible image noise.

The quantification of the retained austenite content was performed by transmission Mössbauer spectroscopy, the informed values are the percentage of austenite in the matrices composed by austenite and martensite. Three samples used in the abrasion test were prepared for Mössbauer experiments, one from each alloy. The samples were cut into $12 \times 12\ \text{mm}$ and $100\ \mu\text{m}$ thick sheets using a wire-erosion machine, brand ActsPark, model PW1, with $200\ \mu\text{m}$ molybdenum wire. After cutting in the EDM, the sheets were glued on a glass slide and had their surface manually sanded with 600 mesh sandpaper until a thickness of $60 \pm 5\ \mu\text{m}$. To carry out the measurements, the samples were detached from the slides. The Mössbauer spectra were obtained in the transmission geometry and in constant acceleration mode, moving a ⁵⁷Co source in Rh matrix from Wissel-GmbH. The photon-counting was performed using a gas proportional counter, and the spectrometer speed was calibrated using a $25\ \mu\text{m}$ Fe-alpha sheet. The spectra were fitted by the least-squares method using NORMOS software¹⁶, assuming simple Lorentzian lines.

The abrasive wear resistance was assessed using a rubber wheel abrasometer with normal brazilian medium-fine 50 mesh, with a 96% 0.15 mm – 0.3 mm granulometry, 97.4% silica content, 0.0 humidity and organic matter < 100 ppm. The samples were washed in an ultrasonic bath using ethyl alcohol and after cleaning, the parts were dried and weighed on an analytical balance and taken to the abrasion machine. The test was carried out with two parameters to verify the behavior of the alloys at different loads. Three specimens of each alloy were tested with the normal constant loads of 45 N and 130 N foreseen in ASTM G65 applied by deadweight against a rubber-coated wheel, rotating with a constant rotation of 215 rpm for 20, 40, and 60 minutes according to Table 3. To determine the volume lost, the material density was determined by the Archimedes method.

Table 1. Chemical compositions of alloys (wt.%).

Alloy	Cr	C	Nb	Mn	Si	Ni	Mo	Cu	P	S
HCCI 0%Nb	26.626	2.892	0.063	1.622	0.572	0.519	0.027	0.088	0.032	0.006
HCCI 0.5%Nb	26.172	2.844	0.476	1.405	0.566	0.498	0.025	0.098	0.032	0.007
HCCI 1%Nb	25.954	2.743	1.014	1.216	0.460	0.488	0.025	0.106	0.034	0.007

The worn surfaces were analyzed using scanning electron microscopy in top view. A sample of each alloy was cut perpendicular of wear direction using a wire-erosion machine, brand ActsPark, model PW1, with 200 μm molybdenum wire.

For statistical analysis, the Microsoft Excel software was used. The ANOVA - Single Factor analysis of variance method was used to compare three populations, rejecting the null hypothesis H_0 for $p < \alpha$ with $\alpha = 0.05$ and $F > F_{\text{critical}}$, indicating that there is a statistically significant difference in at least one pair of means. For comparison between two populations, Student's t-test was used in pairs for means, rejecting the null hypothesis H_0 for $p < \alpha$ with $\alpha = 0.05$.

3. Results and Discussion

The X-ray diffractometry shown in Figure 1 confirms the presence of martensite phase and M_7C_3 carbides from the observed peaks in HCCI0%Nb, HCCI0.5%Nb, and HCCI1%Nb spectra. No $M_{23}C_6$ and M_3C carbide peaks were identified. The three alloys resulted in similar spectra, with the appearance of peaks referring to $NbC_{0.75}$ ¹⁷ constituent in the HCCI1%Nb alloy being highlighted. The $NbC_{0.75}$ XRD peak and BDEC – ICSD files stoichiometry comparison is shown with more details in Figure 2.

These peaks were also expected in the HCCI0.5%Nb alloy which has lower niobium content, but they appear only with a very low intensity, hardly to see in the diffractogram. The peaks at 43° and 50.5° indicate the presence of retained austenite in heat-treated alloys.

Figure 3 shows the alloys microstructures. The HCCI0%Nb alloy (Figure 3a) presented a near-eutectic microstructure, composed of the eutectic formed by the martensitic matrix + secondary carbides (SC) and eutectic M_7C_3 rod-type carbides morphologies; and small fractions of martensite + secondary carbides (SC) originated from the proeutectic austenite formed during solidification.

The rod-type M_7C_3 carbides are identified by number 1. It is observed from Figures 3b and 3c that the addition of niobium changes the microstructure from near-eutectic to hypoeutectic microstructure, resulting in the appearance of dendrites formed by martensite + SC originated from the proeutectic austenite (γ). The modified eutectic's morphology, during the solidification of the alloy, induces the formation of blade-type M_7C_3 carbides¹⁸, identified by number 2. The change in eutectic morphology that results in the appearance of

blade-type carbides is caused by the presence of greater fractions of proeutectic austenite after solidification, which causes smaller undercooling (because of the heat released by the formation of the proeutectic austenite), favoring the blade-like carbide shape formation¹⁸.

In the mappings shown in Figures 4, 5, and 6, the presence of niobium was highlighted by the yellow color, chromium by the blue color, and iron by the red color, thus allowing an analysis of the rich regions of each of the elements and the identification of the $NbC_{0.75}$, M_7C_3 , and matrix carbides. In Figure 4, it can be seen that iron is found mainly in the matrix, while chromium is mainly found in M_7C_3 carbides.

The same analogy can be made in Figures 5 and 6, referring to HCCI0.5%Nb and HCCI1%Nb alloys, respectively. However, the appearance of $NbC_{0.75}$ carbides in petal-like and fine blade-like forms ($NbC_{0.75}$ chinese script morphology) is also observed. This morphology converges with those found in the literature in alloys with similar niobium levels^{4-6,19}.

Three distinct morphologies were observed for the secondary carbides: in smaller quantities, the discrete rods, identified in

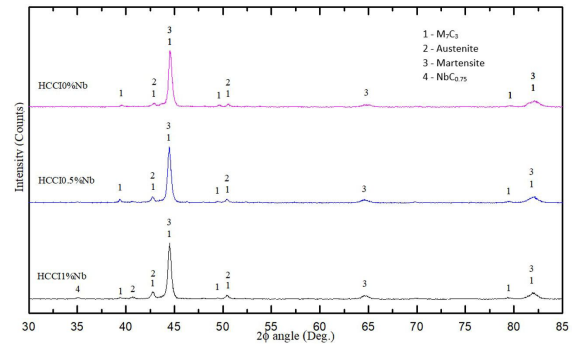


Figure 1. X-ray diffractometry performed on the samples.

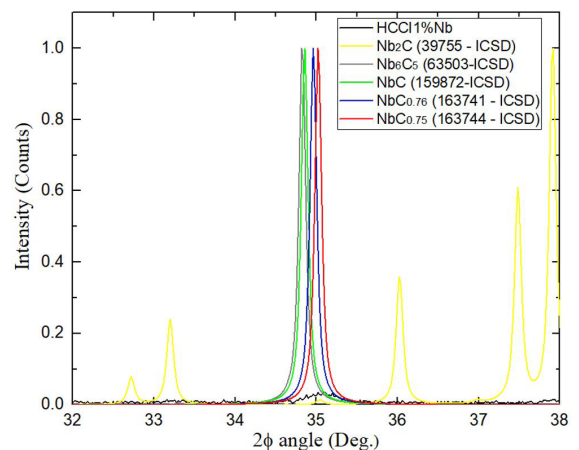


Figure 2. NbC_x XRD peak and BDEC – ICSD files stoichiometry comparison.

Table 2. Phase crystallographic properties.

Phases	ICDD PDF No	Space group
Austenite	00-031-0619	Fm3m (225)
Ferrite*	00-001-1262	Im3m (229)
M_7C_3	00-005-0720	P31c (159)
$NbC_{0.75}$	163744**	Fm3m (225)

(*Ferrite and Martensite have coincident peaks) **ICSD File No

Table 3. Wear test parameters.

	Load (N)	Duration (min)	Granulometry (mesh)	Wheel speed (rpm)	Sand flow (g/min)
Higher load	130	20, 40, 60	50	215	300
Lower load	45	20, 40, 60	50	215	300

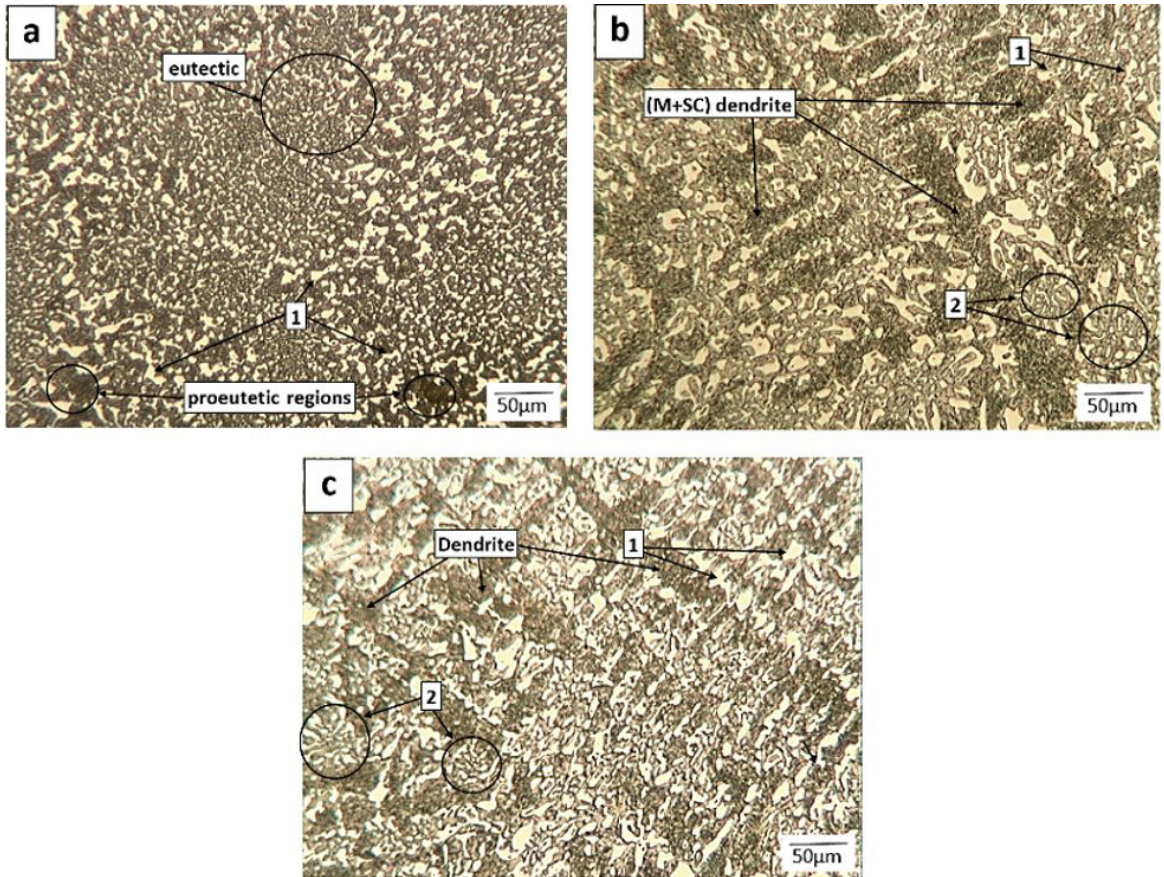


Figure 3. Optical microscopy (a) HCC10%Nb; (b) HCC10.5%Nb; (c) HCC11%Nb. M: Martensite; SC: Secondary Carbides; 1: rods-type M_7C_3 carbides; 2: blade-type M_7C_3 carbides.

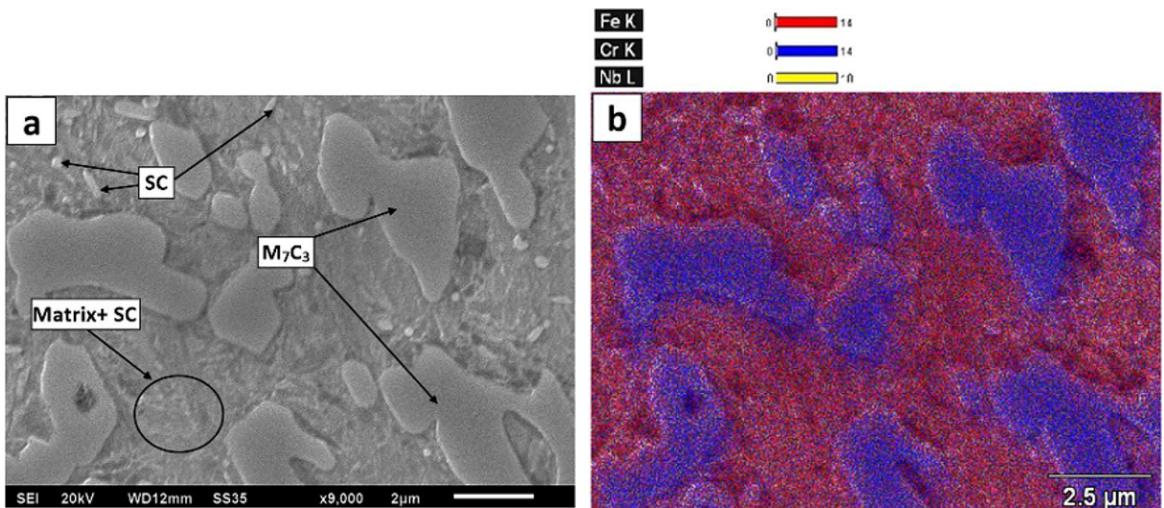


Figure 4. Microstructure of the HCC10%Nb alloy (a) SEM; and (b) chemical mapping.

Figure 6a by the letter “a”, plate-like shapes, identified by the letter “b”, and in larger quantities, the rod-like particles, identified by the letter “c”. These morphologies were found by Powell and LAIRD (1992)²⁰ for secondary carbides of the M_7C_3 type.

The observed morphology and X-ray diffraction rule out the hypothesis of secondary carbides of the M_3C and $M_{23}C_6$ type.

$NbC_{0.75}$ carbides appeared as small colonies (Figure 7), located at interdendritic regions. Although $NbC_{0.75}$ carbides

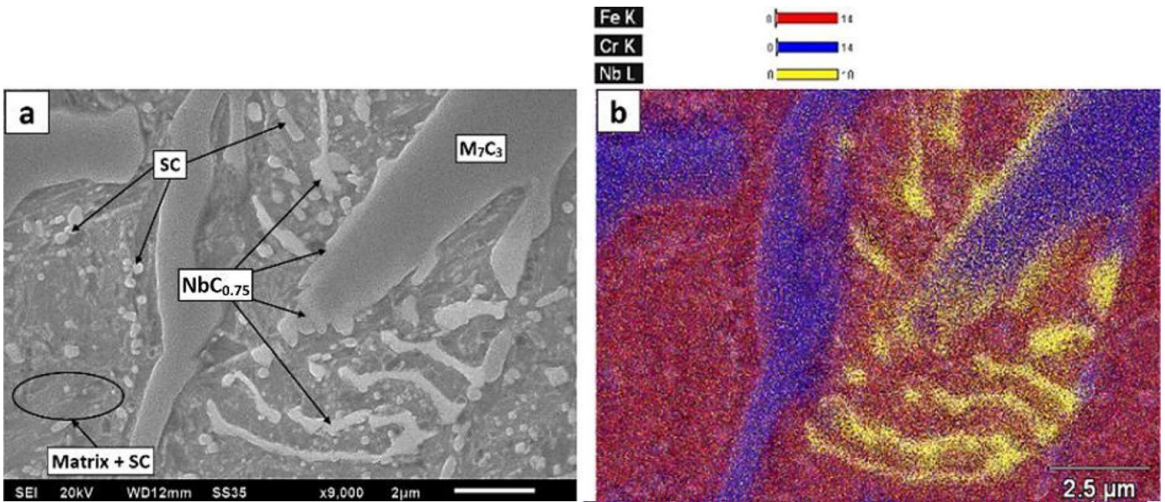


Figure 5. Microstructure of the HCC10.5%Nb alloy (a) SEM; and (b) chemical mapping.

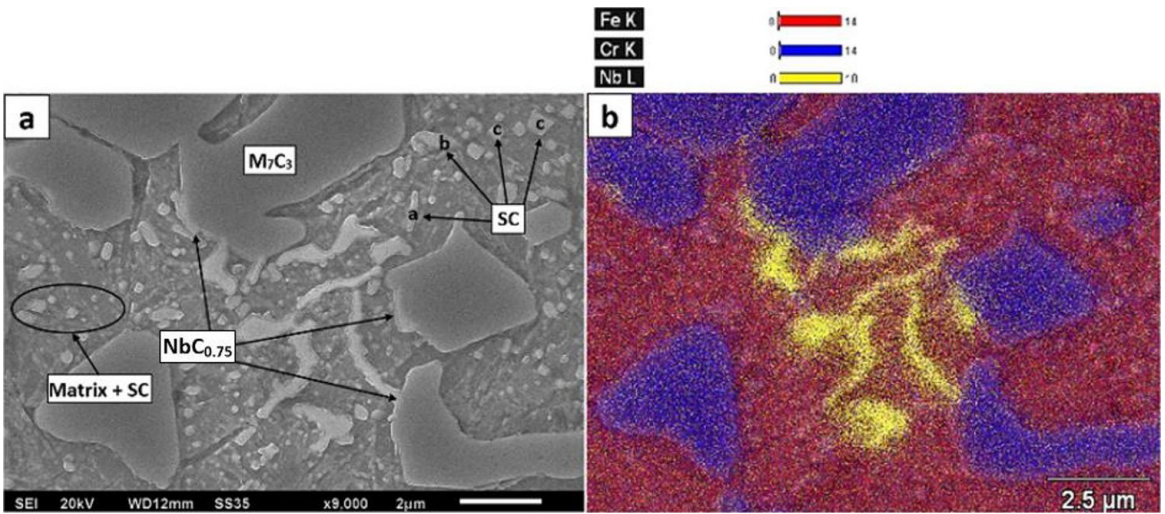


Figure 6. Microstructure of the HCC11%Nb alloy (a) SEM; and (b) chemical mapping.

are frequently reported as nucleating agents for austenite dendrites during solidification^{4,19}, it is also observed in Figures 5 and 6, great proximity between them and the eutectic regions. In the same figures, can be seen in some regions, that the NbC_{0.75} carbides formed a coating of the M₇C₃ carbides and eutectic regions, which may contribute to the abrasive wear resistance increase, acting as a support for greater hardness and better fixation in the matrix for these regions.

In general, high Nb content (upper ~ 5%Nb) in HCCI, promotes first NbC_x solidification²¹⁻²³, and these NbC_x carbides can be nucleation points, however, for smaller Nb content in a hypoeutectic alloy analogous to this paper, Kesri and Durand-Charre²³ found in a 14,7%Cr-2,1%C-1%Nb cooled at 150°C/h⁻¹, the proeutectic austenite solidified first, at around 1332°C, followed by the “chinese script” NbC_x-austenite eutectic at 1232°C and then, M₇C₃-austenite eutectic at 1213°C. Both eutectic NbC_x-austenite and M₇C₃-austenite

formed in interdendritic grooves. The small difference temperature from NbC_x-austenite eutectic and M₇C₃-austenite forming, calls attention (19°C), because in a faster cooling than 150°C/h⁻¹ these constituents can solidify almost together, justifying the proximity from NbC_{0.75} carbides from eutectic regions and M₇C₃ at this work.

The Mössbauer spectra can be seen in Figure 8. It is possible to see three different patterns of curves, six smaller peaks, called sextets, can be noticed represented by pink curves, blue, yellow and orange, two intermediate peaks, called doublets, represented by the green curve, and a larger peak, called singlet also represented by the light blue color. The black curve represents the resulting sum of the curves. The areas under the singlet spectra indicate the low carbon austenite contents, under the doublets the high carbon austenite, and under the sextet, the martensite contents²⁴.

The contents of martensite and of the high and low carbon retained austenite in the matrices are shown in Figure 9.

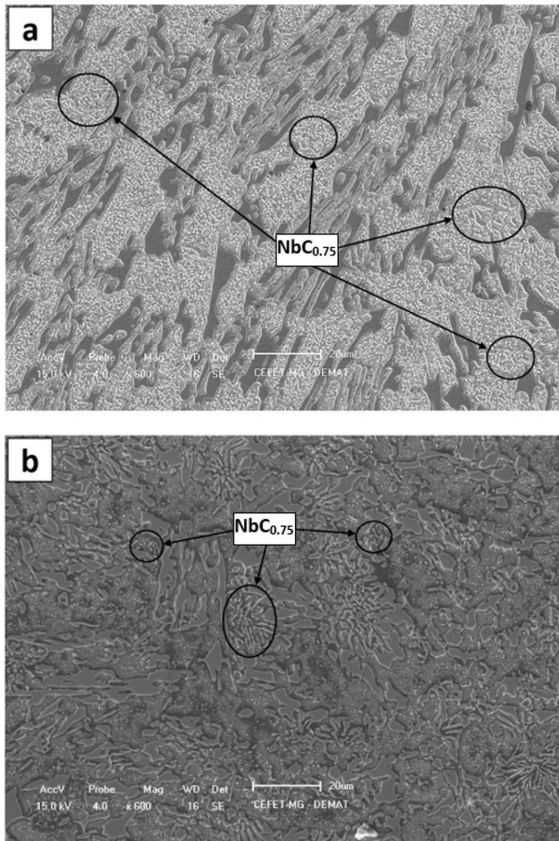


Figure 7. Colonies of $\text{NbC}_{0.75}$ carbides (a) HCCI0.5%Nb; and (b) HCCI1%Nb.

The levels found are of similar magnitude to those obtained by Weber et al.²⁴. The authors²⁴ studied three different alloy (17.5Cr-2.66C, 18.74Cr-2.5C, 23.86Cr-3.07C) fracture toughness and grinding balls wear resistance in function of low and high carbon retained austenite and martensite. It is important to mention about the 23.86Cr-3.07C heat-treated at 1050°C for 4h and 2h at 200°C alloy, analogous to the compositions and heat treatments used in the present work, the authors found 15% of low carbon retained austenite in matrices, and 16% of high carbon retained austenite. This was the highest retained austenite (31%) found in the matrices in this alloy, resulting in the highest fracture toughness and wear resistance in this alloy either.

At this work, the highest total retained austenite content was found in HCCI0.5%Nb (36%), followed by HCCI0%Nb (32%) and HCCI1%Nb (30%). The HCCI0.5%Nb showed higher content of low and high carbon retained austenite, 17% and 19%, respectively. The HCCI1%Nb differed from the HCCI0%Nb because of the high carbon austenite content reduction, 18% comparing to 16%, resulting then in a martensite content increase from 68% to 70%. We could not find any niobium presence and alloy hardenability correlation.

Table 4 shows the alloy hardness, matrix microhardness, total retained austenite content in the matrices, and the microstructural quantifications resulting from image analysis.

The ANOVA variance analyses presented in Table 5 indicate that the niobium addition did not influence the alloys hardness and matrix microhardness. Nonetheless, it caused a reduction in the average size, average perimeter, and volumetric fraction of the carbides.

With the carbides volumetric fraction reduction due to the niobium addition and matrix microhardness maintenance, it

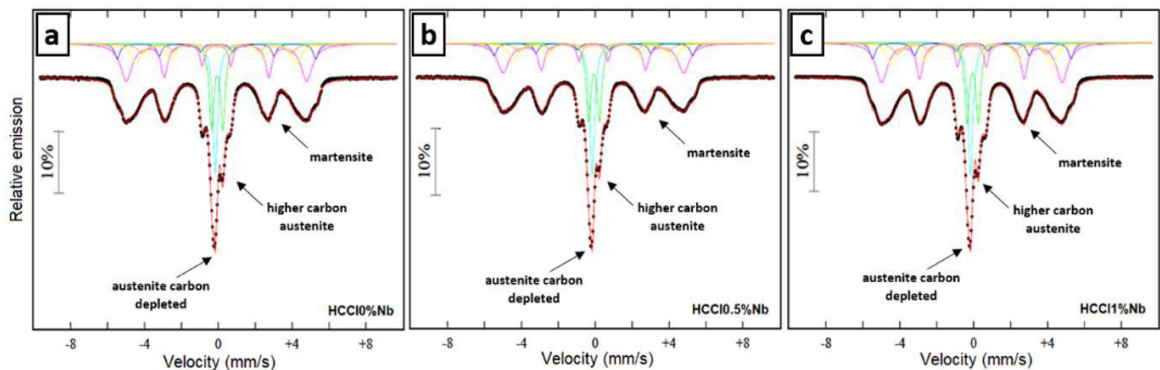


Figure 8. Mössbauer spectra obtained from analyzed samples. (a) HCCI0%Nb; (b) HCCI0.5%Nb; (c) HCCI1%Nb.

Table 4. Properties and microstructural quantifications of the alloys.

Alloy	Hardness (HRC)	Matrix microhardness (HV0.05)	Retained austenite in the matrices (%)	Carbides amount	Carbides average size (μm^2)	Carbides average perimeter (μm)	Carbides volume fraction (%)
HCCI0%Nb	56.4±2.2	610±31	32	514±62	20.8±3.1	30.7±3.3	25.5±2.2
HCCI0.5%Nb	55.5±2.8	600±20	36	472±69	19.7±2.0	28.7±2.3	22.2±1.6
HCCI1%Nb	55.1±3.0	609±13	30	513±27	15.8±1.8	27.1±2.2	19.5±1.7

was expected a decrease in the alloys hardness^{3,18}. However, this variation was not observed. The niobium carbides presence can justify maintaining the hardness level.

ANOVA variance analysis (Table 5) indicates that the niobium addition did not influence the carbides amount with an area greater than $3\mu\text{m}^2$. However, as the carbides amount average in HCCI0.5%Nb alloy decreased considerably, this may have occurred due to the higher retained austenite content in the alloy, indicating less austenite destabilization and consequent smaller number of secondary carbides formed, carbides that are significantly influence the carbide count. Student's t-test was performed for direct comparison between the carbides amount in the alloys. The results can be seen in Table 6.

Student's t-test indicates a reduction in the carbides amount with an area greater than $3\mu\text{m}^2$ after adding 0.5%Nb. It is also noted that there is no statistically significant difference in the carbides amount in the alloy with 1%Nb compared to 0%Nb and 0.5%Nb alloys. The increase in the average carbides amount in the HCCI1%Nb alloy compared to the HCCI0.5%Nb may be due to the lower retained austenite content found, suggesting greater destabilization of austenite and consequently formation of a greater number of secondary

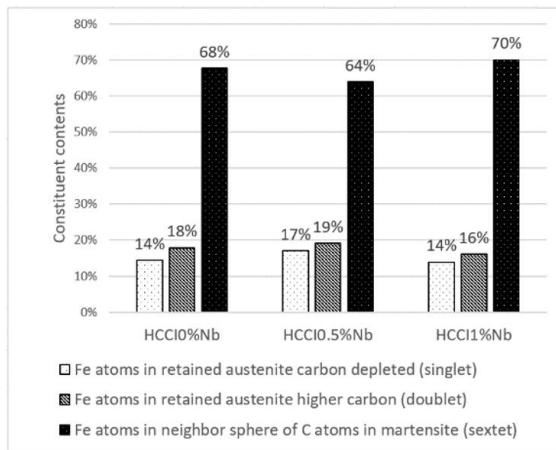


Figure 9. Retained austenite and martensite contents in the matrices obtained by Mössbauer spectroscopy.

carbides. Even with this hypothesis and with the lowest content of retained austenite, the HCCI1%Nb alloy did not present the highest number of carbides amount when compared to the other alloys, because, despite greater destabilization, the reduction of CVF can reduce the carbides amount.

The worn volumes after 60 minutes tests with 130N and 45N loads are shown in Figure 10, and student t-tests performed for statistical comparison are shown in Table 7.

Both 130N and 45N load tests indicated a superior performance for the HCCI0.5%Nb alloy as compared to HCCI0%Nb. The HCCI1%Nb alloy did not show any performance gain when compared to HCCI0%Nb. Moreover, for the HCCI0.5%Nb alloy, even under the most severe wear regime (130N), the volume of removed material was smaller than for HCCI0%Nb under the milder regime (45N).

In the wear tests, interruptions were made every 20 minutes in order to measure the volume loss as a function of time. The tests presented a linear behavior, as shown in Figures 11a and 11b. The fitted linear and angular coefficients b and a , respectively, represent the initial transient regime, called *running-in* and the steady-state wear rate²⁵.

The wear rates obtained from the regressions are shown in Figure 12 along with the volumetric fraction of carbides and retained austenite content in the matrices.

The carbides volumetric fraction reduction and the microstructure transition from eutectic to hypoeutectic could increase the average wear rate of the alloys^{3,18}. However, the

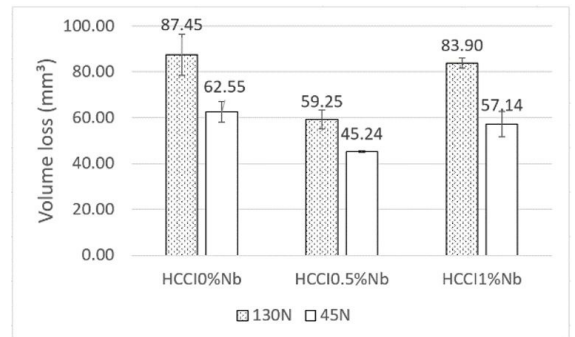


Figure 10. Volume loss after 60 minutes of testing.

Table 5. ANOVA variance analysis of the alloys microstructural properties and quantifications.

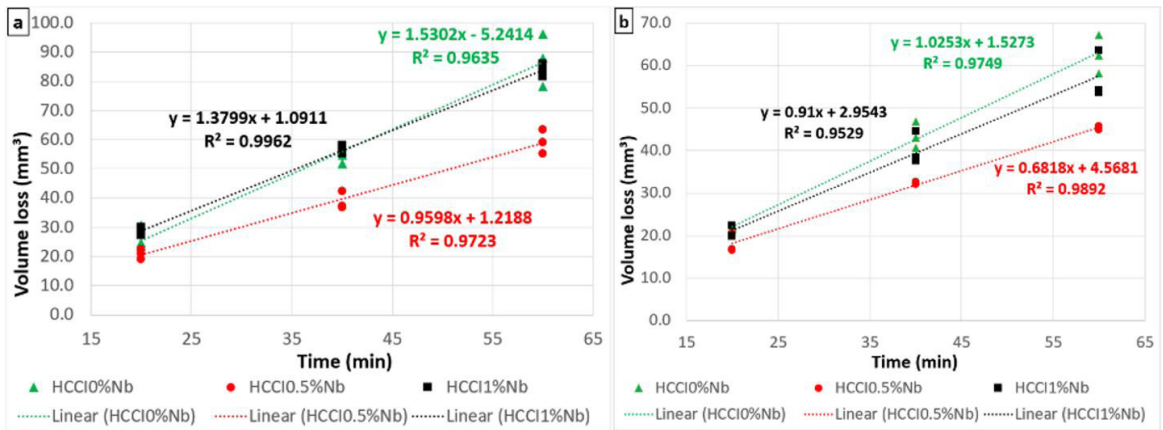
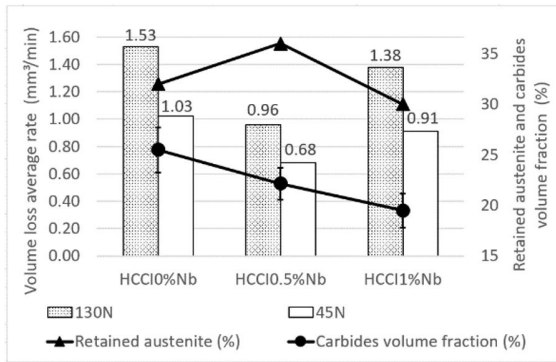
Property	p-value	α	F	F critical	Conclusion
Hardness	0.354	0.05	1.060	3.179	Same
Matrix microhardness	0.582	0.05	0.552	3.354	Same
Carbides amount	0.182	0.05	1.815	3.354	Same
Carbides average size (μm^2)	1.37E-04	0.05	12.585	3.354	Different
Carbides average perimeter (μm)	0.020	0.05	4.534	3.354	Different
Carbides volume fraction (%)	3.85E-07	0.05	26.816	3.354	Different

Table 6. Student's t test for direct comparison between carbides amount.

Alloy	Property	p-value	α	Conclusion
HCCI0%Nb - HCCI0.5%Nb	Carbides amount	0.017	0.05	Different
HCCI0.5%Nb - HCCI1%Nb	Carbides amount	0.126	0.05	Same
HCCI0%Nb - HCCI1%Nb	Carbides amount	0.972	0.05	Same

Table 7. Student's t test of volume losses after 60 minutes of testing.

Alloy	Property	p-value	α	Conclusion
130N				
HCC10%Nb - HCC10.5%Nb	Volume loss	0.010	0.05	Different
HCC10%Nb - HCC11%Nb	Volume loss	0.635	0.05	Same
45N				
HCC10%Nb - HCC10.5%Nb	Volume loss	0.020	0.05	Different
HCC10%Nb - HCC11%Nb	Volume loss	0.317	0.05	Same
45N - 130N				
HCC10.5%Nb (130N) - HCC10%Nb (45N)	Volume loss	0.005	0.05	Different
HCC10.5%Nb (130N) - HCC11%Nb (45N)	Volume loss	0.652	0.05	Same

**Figure 11.** Volume loss curves as a function of time (a) 130N; (b) 45N.**Figure 12.** The relationship between wear rates, CVF and retained austenite in matrices.

HCC10.5%Nb alloy presented an average rate of volume loss 37% lower than the HCC10%Nb alloy in 130N load test and 34% in the 45N test.

The presence of NbC_{0.75} carbides justifies the performance gain. The NbC_{0.75} petal-like shape carbides morphologies observed in HCC10.5%Nb and HCC11%Nb alloys (Figures 5 and 6) result in good fixation in the matrix⁵ and, consequently, greater toughness and wear resistance when compared to M₇C₃ carbides⁴.

The NbC_{0.75} carbides high hardness (~2400 - 3000HV0.05)⁸ and their favorable morphology⁵ makes them act effectively in interrupting wear micromechanism, protecting

the matrix and preventing M₇C₃ carbides pulling. In addition, the NbC_{0.75} layers formed around some M₇C₃ carbides found in niobium-rich regions and shown in Figures 5 and 6 can also hamper the chipping and cracking M₇C₃ carbides processes.

From Student's t-tests of the final worn volumes it was not possible to establish that there was a performance gain in the HCC11%Nb alloy compared to HCC10%Nb. According to Zum Gahr and Eldis (1980)³, the volumetric loss variation curve in the rubber wheel test has a convex profile as a function of the carbides volumetric fraction, with the eutectic region being the minimum point region, in other words, distant regions from the eutectic region have the wear resistances more sensitive to carbides volumetric fraction variation than the regions close to the eutectic. Figure 13 illustrates a possible positioning of the HCC10%Nb, HCC10.5%Nb, and HCC11%Nb alloys in a adapted curve from Zum Gahr and Eldis³.

The results suggest that the carbides volumetric fraction reduction influence in wear resistance was more steep when comparing the HCC10%Nb alloy with the HCC11%Nb than in the comparison between HCC10%Nb and HCC10.5%Nb. Thus, the niobium addition beneficial effects in HCC11%Nb may have been sufficient only to compensate this reduction, since the HCC11%Nb alloy is further from the eutectic region, in other words, the volumetric loss is more sensitive to the carbides volumetric fraction variation than eutectic closest alloys (HCC10.5%Nb and HCC10%Nb).

The highest retained austenite content was found in the HCC10.5%Nb (see Table 4), indicating 36% content, that is,

the one that presented the best performance for both 45N and 130N wear tests. The HCCI0%Nb and HCCI1%Nb alloys

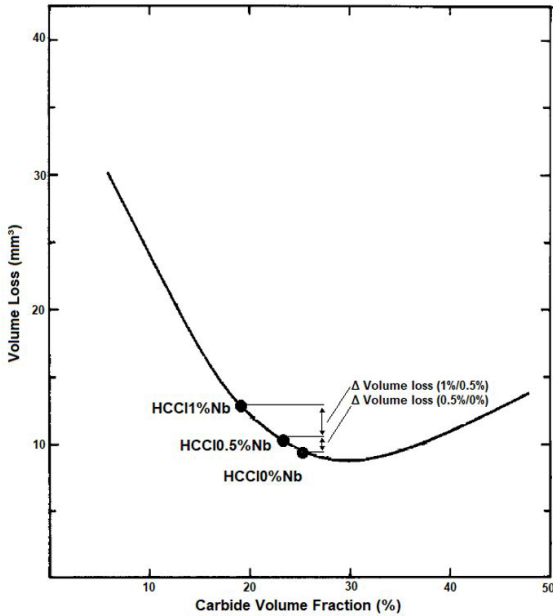


Figure 13. Positioning of alloys in an adapted curve by Zum Gahr and Eldis (1980)*. *The positioning illustrates the alloys expected behavior, disregarding $NbC_{0.75}$ carbides effect. The magnitude of worn volumes cannot be directly compared to the present work due to variations between test parameters, such as time, size, and abrasive shape.

resulted in 32 and 30% respectively of retained austenite with statistically equal wear rates. The retained austenite presence in greater proportion may have caused a positive influence on the HCCI0.5%Nb performance due to its hardening capacity, martensite formation by deformation during the abrasive penetration, and an alloy toughness increase.

The worn surfaces are shown in Figure 14, with Figures (a), (b), and (c) the alloys HCCI0%Nb, HCCI0.5%Nb, and HCCI1%Nb worn with a 130N load and (d), (e), and (f) at 45N, respectively.

Figure 14 shows the appearance of grooves in all alloys, both in the 130N and 45N tests, which are better defined in the first condition (more severe). The HCCI0%Nb alloy showed more intense grooves and HCCI0.5%Nb less intense ones, indicating an inverse relationship between microcutting and abrasive wear resistance. The HCCI0.5%Nb alloy differs from the others, both in 30N and 45N load tests, by the appearance of timid grooves and pits, which are not observed in the HCCI0%Nb and HCCI1%Nb alloys. For a constant abrasive flow, the transition from the wear regime of grooving abrasion to rolling abrasion occurs by reducing the load, resulting in pits' appearance²⁶. However, it was not possible to observe a higher concentration of pits in the 45N test (Figure 14e) compared to the test with 130N (Figure 14b). $NbC_{0.75}$ carbides may have acted as barriers to abrasive penetration, acting together with M_7C_3 carbides as microcutting switches and causing intermittently abrasive roll, justifying the mixed appearance of grooves and pits in the HCCI0.5%Nb alloy. The large proeutectic austenite increase observed in the HCCI1%Nb alloy may have acted

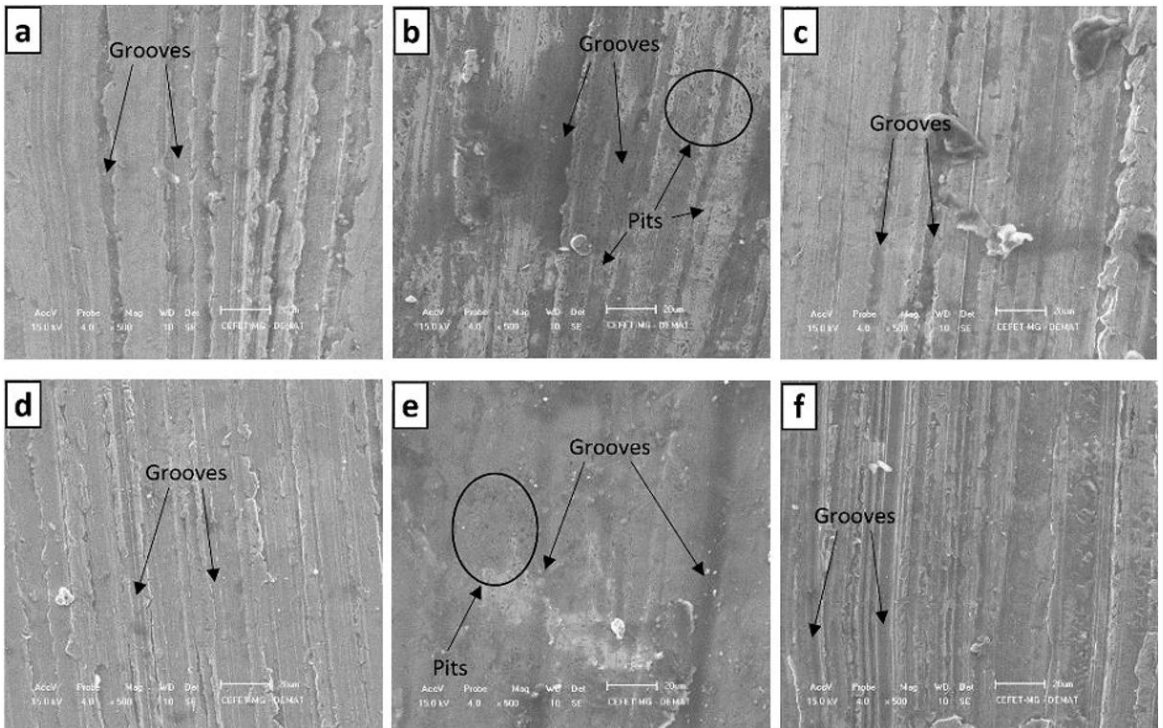


Figure 14. Scanning electron microscopy of the top view of the worn surfaces at 130N (upper line) and 45N (lower line): (a, d) HCCI0%Nb; (b, e) HCCI0.5%Nb; (c, f) HCCI1%Nb.

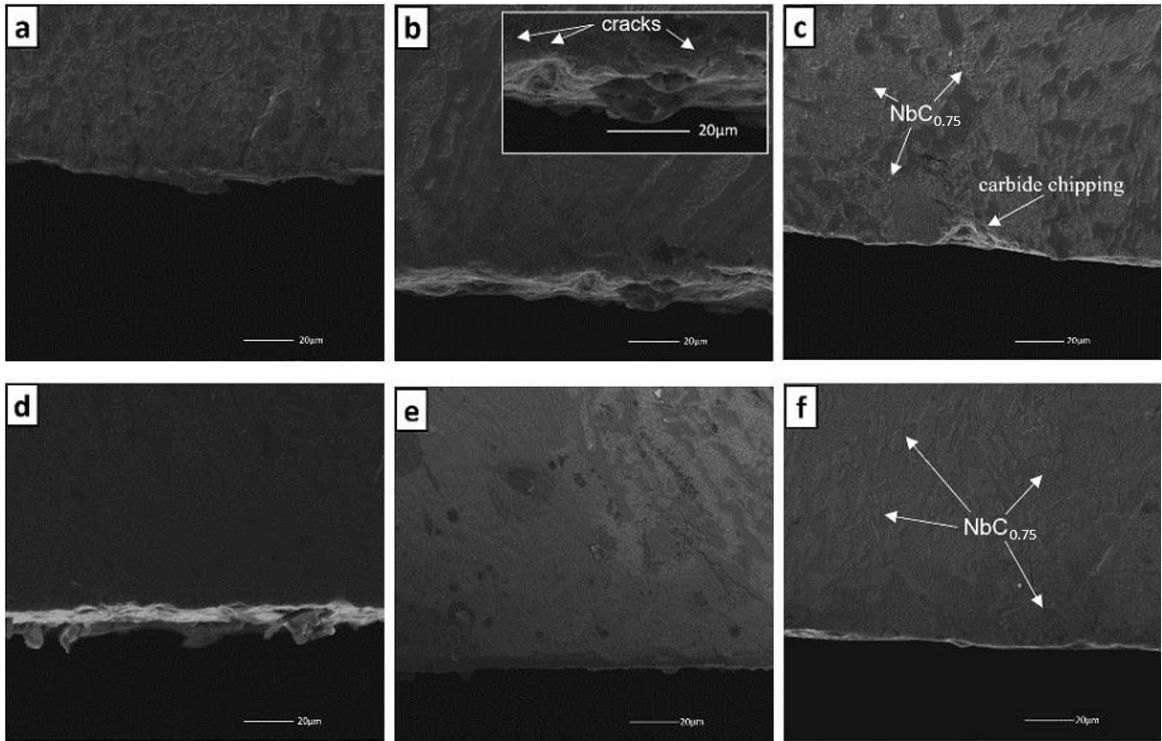


Figure 15. Cross-sectional scanning electron microscopy at 130N (upper line) and 45N (lower line): (a, d) HCCI0%Nb; (b, e) HCCI0.5%Nb; (c, f) HCCI1%Nb.

oppositely, facilitating abrasive penetration justifying the non-appearance of pits, even with the $\text{NbC}_{0.75}$ carbides presence.

The cross-sectional surfaces are shown in Figure 15, with Figures (a), (b), and (c) the alloys HCCI0%Nb, HCCI0.5%Nb, and HCCI1%Nb worn with a 130N load and (d), (e), and (f) at 45N, respectively.

Figure 15 shows a greater irregularity of surfaces in 130N tests when compared to 45N condition in all alloys. In the HCCI1%Nb alloy (Figure 15c), it was possible to observe carbide chipping regions with low frequency. It is believed that the increase in the fraction of matrix originating from proeutectic austenite dendrites may have favored the penetration of the abrasive in these regions and favoring any chipping. Micro-cracks were also found at low frequency in the HCCI0.5%Nb alloy (Figure 15b). Their appearance may have occurred due to small possible vibrations generated during the rolling of abrasives between the wheel and the worn surface. The presence of microcracks suggests the occurrence of material removal by brittle fracture and a consequent substantial increase in the wear rate²⁵. However, small microcracks amount were observed in the present work, with no significant removal by brittle fracture.

4. Conclusion

The niobium addition changed the microstructure from near-eutectic to hypoeutectic and reduced the average size, average perimeter, and volumetric fraction of the carbides.

A close proximity between $\text{NbC}_{0.75}$ and eutectic carbides was detected in the alloys with 0.5%Nb and 1%Nb, and in

some regions, the $\text{NbC}_{0.75}$ carbides formed a coating around the M_7C_3 carbides and eutectic regions, which may have contributed to increased resistance to abrasive wear, serving as a support for greater hardness and better fixation in the matrix for these regions.

The 0.5%Nb alloy showed higher levels of retained austenite high and low carbon in the matrices, 17% and 19%, respectively, compared to the other alloys. The 0%Nb and 1%Nb alloys showed the same low-carbon retained austenite, 14%, while high carbon retained austenite was found to be 18% and 16%, respectively.

The 0.5%Nb alloy showed the best performance in the rubber wheel abrasive wear tests, with a average volume loss rate 37% lower than the without niobium addition alloy in the test with 130N load and 34% in the 45N test. Even in a more severe wear (130N) regime, the 0.5%Nb alloy had a lower material volume removed than the alloy without niobium in a milder regime (45N). The performance gain may be caused by cold work hardening and favorable $\text{NbC}_{0.75}$ morphology and hardness.

Less intense grooves and the appearance of pits in the alloy with greater resistance to abrasive wear (0.5%Nb) were observed.

There was no performance gain in the abrasive wear resistance of the 1%Nb alloy compared to the alloy without niobium addition. Nonetheless, they both showed statistically equal volumetric losses even with the reduction of the carbide volume fraction of 25.51% of the alloy without niobium addition to 19.49% of the alloy with 1% niobium.

Hypoeutectic microstructure with niobium addition (0.5%Nb) has greater wear resistance when compared to the near-eutectic one, however, the performance gain from niobium addition of can be canceled as the microstructure moves further away from the near-eutectic microstructure (1%Nb).

5. Acknowledgments

This work was conducted with the support of the Coordination for the Improvement of Higher Education Personnel - Brazil (CAPES) - Financing Code 001, the Federal Center of Technological Education of Minas Gerais (CEFET-MG) and Instituto Federal de Minas Gerais (IFMG). The authors also acknowledge the financial support from the Brazilian Agencies CNPq and FAPEMIG.

6. References

- Zum Gahr KH. Microstructure and wear of materials. Amsterdam: Elsevier; 1987. (vol. 10).
- Laird G, Gundlach R, Rohrig K. Abrasion-resistant cast iron handbook. Schaumburg, IL: American Foundry Society; 2000.
- Zum Gahr KH, Eldis GT. Abrasive wear of white cast irons. *Wear*. 1980;64(1):175-94.
- Filipovic M, Kamberovic Z, Korac M, Jordovic B. Effect of niobium and vanadium additions on the as-cast microstructure and properties of hypoeutectic Fe–Cr–C alloy. *ISIJ Int*. 2013;53(12):2160-6.
- Chen HX, Lu JC, Lin HT. Effect of niobium on wear resistance of 15%Cr white cast iron. *Wear*. 1993;166(2):197-201.
- Penagos JJ, Pereira JI, Machado PC, Albertin E, Sinatora A. Synergetic effect of niobium and molybdenum on abrasion resistance of high chromium cast irons. *Wear*. 2017;376–377:983-92.
- Woydt M, Mohrbacher H, Vleugels J, Huang S. Niobium carbide for wear protection – tailoring its properties by processing and stoichiometry. *Met Powder Rep*. 2016;71(4):265-72.
- Woydt M, Huang S, Vleugels J, Mohrbacher H, Cannizza E. Potentials of niobium carbide (NbC) as cutting tools and for wear protection. *Int J Refract Met Hard Mater*. 2018;72:380-7.
- Silva AE, Melo INR, Pinheiro IP, Silva LR. Characterisation and machinability of high chromium hardened white cast iron with and without the addition of niobium. *Wear*. 2020;460-461:203463.
- Filipovic M, Kamberovic Z, Korac M, Gavrilovski M. Microstructure and mechanical properties of Fe–Cr–C–Nb white cast irons. *Mater Des*. 2013;47:41-8.
- Guesser WL, Costa PHC, Pieske A. Niobium additions in white cast irons alloyed with chromium, for applications at high load abrasive wear [Internet]. São Paulo: Associação Brasileira de Metais; 1989 [cited 2021 Nov 2]. Available from: <https://www.osti.gov/etdweb/biblio/633685>
- Máscia R. Development and tribological characterization of abrasive wear resistant materials for the cassiterite mining industry. Uberlândia: Federal University of Uberlândia; 2022.
- Bouhamla K, Hadji A, Maouche H, Merradi H. Effet du niobium sur la résistance à l'usure d'une fonte au chrome traitée thermiquement. *Metall Res Technol*. 2011;108(2):83-8.
- Silva AE, Melo INR, Pinheiro IP, Silva LR. Influence of Niobium addition on microstructure and machinability of high chromium cast iron. *Mater Res*. 2021;24(5):e20200429. <http://dx.doi.org/10.1590/1980-5373-mr-2020-0429>.
- Tabrett CP, Sare IR, Ghomashchi MR. Microstructure-property relationships in high chromium white iron alloys. *Int Mater Rev*. 1996;41(2):59-82.
- Brand RA. Normos-90 Mössbauer fitting program package. Duisburg: Lab Angewandte Phys, Universität Duisburg; 1994. 8 p.
- Skrípov AV, Wu H, Udovic TJ, Huang Q, Hempelmann R, Soloninin AV, et al. Hydrogen in nonstoichiometric cubic niobium carbides: neutron vibrational spectroscopy and neutron diffraction studies. *J Alloys Compd*. 2009;478(1):68-74.
- Doğan N, Hawk JA, Laird G 2nd. Solidification structure and abrasion resistance of high chromium white irons. *Metall Mater Trans, A Phys Metall Mater Sci*. 1997;28(6):1315-28.
- Ibrahim MM, El-Hadad S, Mourad M. Enhancement of wear resistance and impact toughness of as cast hypoeutectic high chromium cast iron using niobium. *Int J Cast Met Res*. 2018;31(2):72-9.
- Powell GLF, Laird G 2nd. Structure, nucleation, growth and morphology of secondary carbides in high chromium and Cr-Ni white cast irons. *J Mater Sci*. 1992;27(1):29-35.
- Correa EO, Alcântara NG, Tecco DG, Kumar RV. Desenvolvimento de ligas ferrosas para solda de revestimento duro auxiliado por simulações termodinâmicas. *TMM*. 2008;4(3):13-7.
- Correa EO, Alcântara N, Tecco D, Kumar R. The relationship between the microstructure and abrasive resistance of a hardfacing alloy in the Fe-Cr-C-Nb-V system. *Metall Mater Trans, A Phys Metall Mater Sci*. 2007;38(8):1671-80.
- Kesri R, Durand-Charre M. Phase equilibria, solidification and solid-state transformations of white cast irons containing niobium. *J Mater Sci*. 1987;22(8):2959-64.
- Weber K, Regener D, Mehner H, Menzel M. Characterization of the microstructure of high-chromium cast irons using Mössbauer spectroscopy. *Mater Charact*. 2001;46(5):399-406.
- Hutchings I, Shipway P. Tribology: friction and wear of engineering materials. Oxford: Butterworth-Heinemann; 2017.
- Trezona RI, Allsopp DN, Hutchings IM. Transitions between two-body and three-body abrasive wear: influence of test conditions in the microscale abrasive wear test. *Wear*. 1999;225:205-14.